CHEMISTRY OF MATERIALS

Open Access

pubs.acs.org/cm

Article

Unveiling the Key Role of Aggregation in the Self-Doping of Conjugated Polyelectrolytes

Fernando Muñoz-Alba, Lorenzo Soprani, Benedetta Maria Squeo, Mariacecilia Pasini, Raúl González-Núñez, Rocío Ponce Ortiz, M. Carmen Ruiz Delgado,* Luca Muccioli,* and Barbara Vercelli*

Cite This: *Chem. Mater.* 2026, 38, 808−818

Read Online

ACCESS | Metrics & More | Article Recommendations | Supporting Information

ABSTRACT: Conjugated polyelectrolytes (CPEs) are a distinct class of polymers that feature a π-conjugated backbone and pendant ionic groups, which confers them unique properties. In particular, since the discovery, during their purification in water, that some CPEs have the ability to be self-doped, they have attracted increasing interest from the organic electronics community. More recently, a self-acid doping mechanism was proposed after it was proven that the degree of doping can be modulated by the addition of an acid or a base. However, the explanation of both the self-doping and self-acid doping processes remains ambiguous, and their investigation continues to present significant challenges. In this work, we address the problem through a combination of experimental and computational techniques, including spectroscopy (UV−vis and Raman) and electrochemistry measurements in conjunction with DFT calculations and molecular dynamics simulations. We performed a comprehensive investigation into the self-doping mechanism of **CPE-2K**, poly [2,6-(4,4-bis-potassium butanylsulfonate-4*H*-cyclopenta-[2.1-b:3,4-b′] dithiophene)-alt-4,7-(2,1,3-benzothiazole)], and its homologue with only one alkyl ionic chain, **CPE-K**. Our findings point to a framework that integrates the self- and self-acid doping mechanisms into a unified one, in which backbone aggregation acts as the driving force.

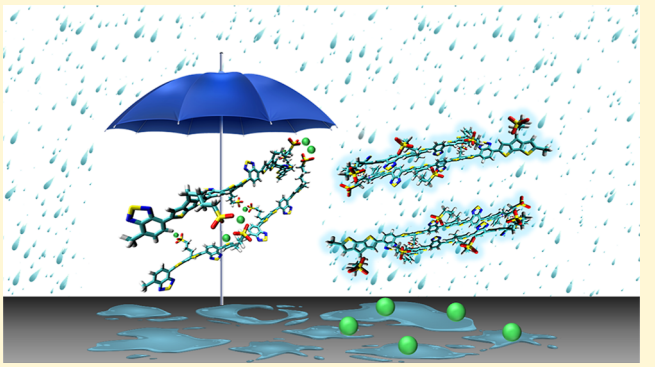

1. INTRODUCTION

Conjugated polyelectrolytes (CPEs) are a unique class of polymers containing a π-conjugated backbone and pendant ionic functionalities, which make them soluble in water and polar solvents.[1,2] CPEs combine the optical and charge transport properties of organic semiconductors with the possibility of modulating their physico-chemical properties by controlling electrostatic interactions.[3] Furthermore, the solubility in water and in polar solvents makes CPEs appealing materials for a wide variety of bioapplications such as biosensors or bioimaging,[4−6] as well as optoelectronic applications such as organic photovoltaic devices,[7−16] light-emitting diodes,[17] organic field-effect transistors,[18−21] actuators, and organic thermoelectrics.[22−24] Recently, the CPE poly[2,6-(4,4-bis-potassium butanylsulfonate-4*H*-cyclopenta-[2.1-b:3,4-b′]dithiophene)-alt-4,7-(2,1,3-benzothiazole)] (PCPDTBT-2SO_3K, or **CPE-2K** for short, see Figure 1) has become an object of interest and study by the research community as it has shown the ability of self-doping during its purification by dialysis in water.[25] It should be noted that this compound has previously been referred to as **CPE-K** in the relevant literature.[3,26] In the present study, the term **CPE-2K** is instead employed for the purpose of distinguishing it from its monosubstituted analog, here called **CPE-K**, as outlined in Figure 1.

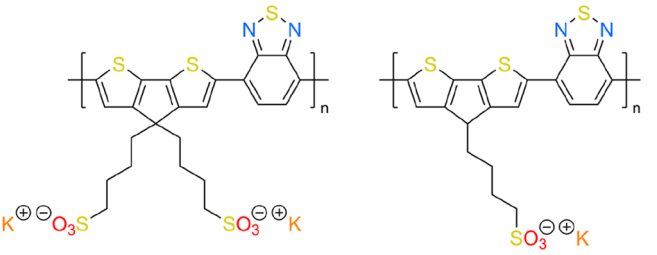

Figure 1. Structures of the studied PCPDTBT polyconjugated polyelectrolytes: **CPE-2K** (left) and **CPE-K** (right).

In particular, it was observed that **CPE-2K** becomes doped in the presence of a proton source and is dedoped with the

Received: September 19, 2025
Revised: December 28, 2025
Accepted: January 5, 2026
Published: January 14, 2026

Scheme 1. Schemes of (a) Electrochemical Self-Doping and (b) Self-Acid-Doping

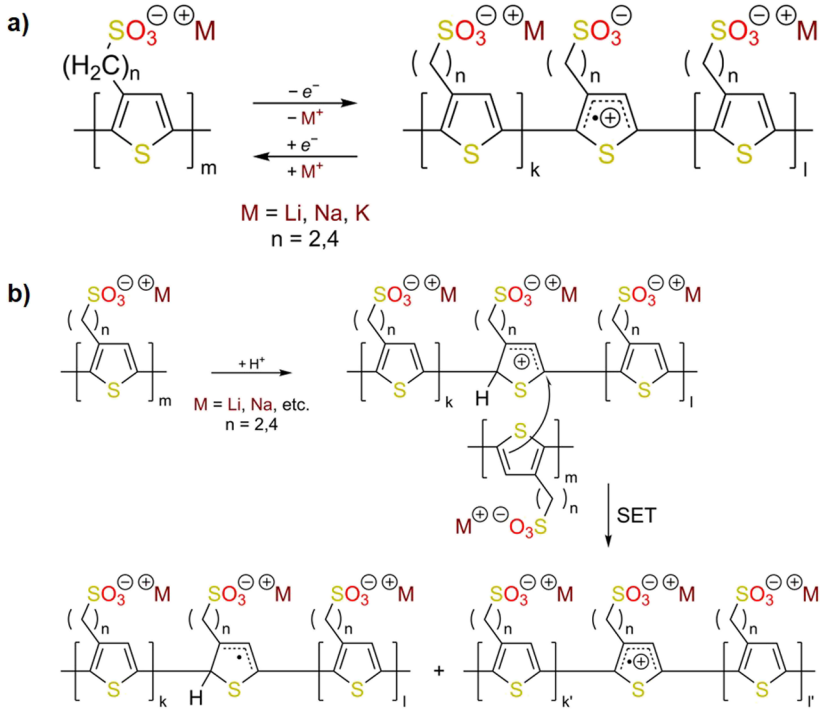

[a]SET stands for single electron transfer.

addition of a base.[25,26] This behavior enables the easy tuning of the doping level by simply adding the desired amount of acid or base: an important feature since precise control of doping is central to modern electronics.

The concept of electrochemical self-doping capability of a polymer was introduced in 1988 by Heeger et al.,[27] who defined "self-dopable" those polymers where the dopants are covalently bonded to their side chains. In particular, in electrochemical studies on the sodium salts and acids of poly(thiophene alkanesulfonates), they observed that the electron ejection from the polymer π-system (positive charging of the backbone) was compensated by proton or other monovalent cation (M^+) concomitant migration to the electrolytic solution, leaving behind a covalently bonded anion (Scheme 1a).

Two years later, Ikenoue et al.,[28] in their studies on poly(thiophene propane sulfonate), found that the acid form of the polymer could show an extremely highly doping level, depending on the degree of dissociation of sulfonic acid groups into sulfonates in the aqueous polymer solution. This phenomenon was defined by Chen and Hua[29] as "self-acid-doping" to distinguish it from the electrochemical self-doping reported by Heeger et al.[27] In the proposed "self-acid-doping" mechanism, the protonation of the polymer backbone induces single-electron transfer (SET) between polymer chains, leading to the formation of the polaron and a transient protonated species, as shown in Scheme 1b.

Concerning the case of **CPE-2K**, the self-doping mechanism proposed in the literature appears to be somewhat unclear. A preliminary work[25] indicates that the phenomenon may be analogous to the mechanism reported in previous research on self-doped polymers. This involves an initial protonation of the polymer backbone, followed by comproportionation with a nonprotonated chain. This process leads to the formation of polarons (radical cations), which are stabilized by anionic pendants. In that case, the anionic nature of the pendants and not the type of the functional group is considered important for the stabilization of the (cationic) polaronic states, which is supposed to be a result of Coulombic stabilization. The second recent work[26] suggests that the nature of the functional groups of the pendants could also play a crucial role in the **CPE-2K** self-doping mechanism. In particular, it highlighted the importance of the sulfonate groups in stabilizing the polymer radical cation and their effect on charge transport and mobility.

However, there are aspects of the proposed mechanism that require further clarification. The protonation is more likely to occur in the sulfonate group than in the polymer backbone, which forms an unstable carbocation that is highly reactive. Furthermore, the second step of the mechanism is a single-electron transfer from another polymer backbone,[30,31] so the distance between different polymer units will play a crucial role in the formation of the polaron and this is not considered in the model.

Taking all these factors into account, here, we present a spectroscopic and electrochemical investigation of **CPE-2K** and its homologue bearing one alkyl ionic pendant PCPDTBT-SO_3K, named as **CPE-K** (Figure 1), combined with a comprehensive theoretical analysis that links density functional theory (DFT) and molecular dynamics (MD) simulations. This combined experimental and theoretical study helps shed light on the self-doping mechanism for this family of CPEs, highlighting the key role of aggregation.

2. EXPERIMENTAL AND COMPUTATIONAL METHODS

UV−vis spectra were collected with a PerkinElmer Lambda 35 spectrometer. Electrochemistry was performed at room temperature in acetonitrile under nitrogen in a three electrodes cell. The counter electrode was platinum; the reference electrode was Ag/Ag^+ (0.1 M

https://doi.org/10.1021/acs.chemmater.5c02392
Chem. Mater. 2026, 38, 808−818

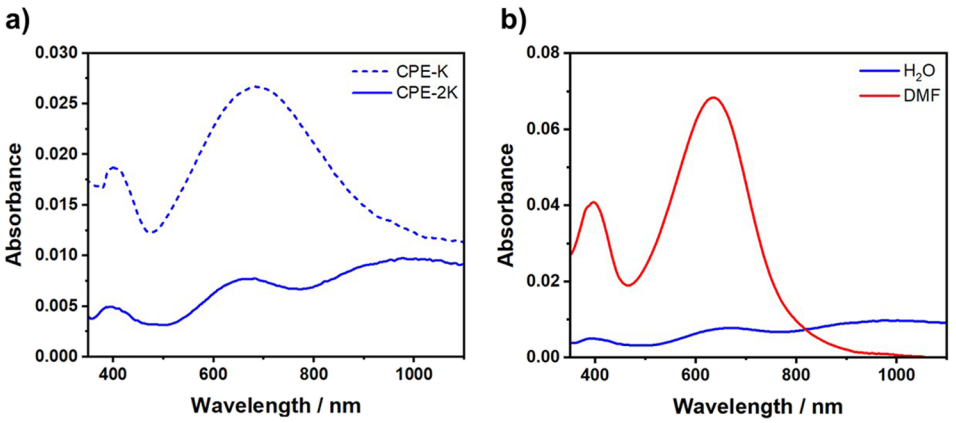

Figure 2. Experimental UV−vis spectra of **CPE-2K** (solid line) and **CPE-K** (dashed line) in water (a) and UV−vis spectra of **CPE-2K** in water and DMF (b). The polymer concentration was 0.025 mg mL^{-1} for all samples.

$AgNO_3$ in acetonitrile, 0.34 V vs SCE, −4.73 V vs vacuum); and the supporting electrolyte was 0.1 M tetrabutylammonium perchlorate (TBAP). Polymers films were cast (ca. 2 μL) onto electrodes at 80−90 °C from 2 mg mL^{-1} solutions in water. The voltammetric apparatus was a Metrohm Autolab 128N potentiostat/galvanostat. The working electrode for cyclic voltammetry (CV) was a glassy-carbon (CG) minidisc electrode (0.2 cm^2).

Raman spectroscopy measurements at 532 and 633 nm were conducted at the Micro-Raman Senterra, a dispersive Raman microscope equipped with a CCD camera; and FT-Raman spectra were recorded by using a JASCO RFT-6000 equipped with an InGaAs detector, a confocal microscope with a 10× objective, and a Nd/YAG laser with excitation at λ = 1064 nm.

Molecular dynamics (MD) simulations of **CPE-K** and **CPE-2K** in dimethylformamide (DMF) and water as solvents were run maintaining a constant pressure of 1 atm, controlled by a Langevin piston,[32] and a constant temperature of 300 K, controlled by velocity rescaling. The simulations were performed under periodic boundary conditions using the NAMD2 software[33] with a time step of 1 fs. Long electrostatic contributions were evaluated using the Particle Mesh Ewald (PME) method,[34] with a 1.5 Å grid spacing.

Stretching and bending parameters were based on the CHARMM force field,[35] while torsion dihedral angles between cyclopentadithiophene (CPDT) and benzodithiophene (BT) were reparametrized from the energy profiles of a DFT-relaxed scan computed at the PBE0-D3/6-31+G** level of theory.[36−38] Atomic charges were calculated at the same level of theory with the ESP fit method.[39]

First, 0.5 ns simulations were carried out for single **CPE-K** and **CPE-2K** monomers in water and DMF to observe the behavior of the K^+ atoms in different solvents. Then, to study the intermolecular interactions, we performed 10 ns simulations with two tetramers of **CPE-K**/**2K** in both solvents. We also simulated the effect of the pH and the countercation size by replacing the K^+ atoms with H^+ and the tetrabutylammonium cation (TBA^+), respectively.

To quantitatively investigate the differences in polaron stabilization between **CPE-K** and **CPE-2K** in water, we performed a simulation, gradually increasing the temperature up to 2000 K to generate some aleatory conformations as random starting positions for other ten additional simulations at 300 K. These simulations had two phases: 20 ns of equilibration and 20 ns of production of results, all with a time step of 1 fs.

The Coulombic stabilization energy per monomer was estimated by summing the contribution of all sulfonate−BT and sulfonate−CPDT pairs, using eq 1, and then dividing E_{coul} by the number of monomer units. A relative dielectric permittivity ε_r = 3 was applied to account for the poor screening provided by water confined in nanometric cavities, where bulk dielectric behavior is not applicable, and for the short distances r_{BS} between the backbones and the sulfonate groups. The charge of the two backbone centers of mass was set to q_B = 0.5 *e*, so the net charge of each backbone monomer was +1 *e*. The sulfonate charges were set to q_S = −1 *e*.

$$E_{coul} = \frac{1}{4\pi\varepsilon_0\varepsilon_r}\sum_{B,S}\frac{q_B q_S}{r_{BS}} \quad (1)$$

In order to calculate the vibrational Raman spectrum, DFT geometry optimization of a monomer of **CPE-2K** was performed at the PBE0-D3/6-31G** level of theory. Note that the alkyl chains were replaced by methyl groups to reduce the computational cost. Dimer models made of two **CPE-2K** monomers in parallel and antiparallel conformations were also optimized at the same level of theory in neutral and radical cation states, aiming to calculate the dimer interaction energy ($E_{dimer} - 2E_{mon}$) and the ionization potential ($E_{cation} - E_{neutral}$).

3. RESULTS AND DISCUSSION

In order to analyze the capability of **CPE-K** and **CPE-2K** to form polaronic species UV−vis spectroscopy was recorded in water,[20] a solvent in which they are soluble owing to the ionic nature of the sulfonate side groups. In fact, the absorption spectrum of **CPE-2K** in water (Figure 2a) displays, besides the two absorption peaks at 395 and 659 nm, attributed to the $\pi-\pi^*$ absorption of the localized π orbitals and the intramolecular charge transfer (ICT) band, respectively,[22,23] a third broad band whose maximum intensity is around 950 nm and extending beyond 1100 nm. This band is ascribed, as demonstrated below, to the formation of positive polarons on the polymer backbone through self-doping.[25]

CPE-K also features the same $\pi-\pi^*$ and ICT bands, although shifted 10 and 30 nm toward lower energies, respectively. However, a notable distinction in the intensity of the polaron band emerges between the two polymers in water. The relative intensity ratio ($A_{Polaron}/A_{ICT}$) is reduced in **CPE-K** compared to that in **CPE-2K**, with values of 0.46 and 1.42, respectively, suggesting a higher polaron stabilization for **CPE-2K** with respect to **CPE-K**. This difference is particularly intriguing since the polaron is formed in the backbone of the conjugated system, and both **CPE-K** and **CPE-2K** possess identical backbones (Figure 1). In order to understand this effect, we discuss in the next sections the influence of different factors (*i.e.*, solvent nature, pH, number of side chains, countercation nature) on the doping process, with the aim of fully addressing the analysis of doping capacity with the number of alkyl chains.

https://doi.org/10.1021/acs.chemmater.5c02392
Chem. Mater. 2026, 38, 808−818

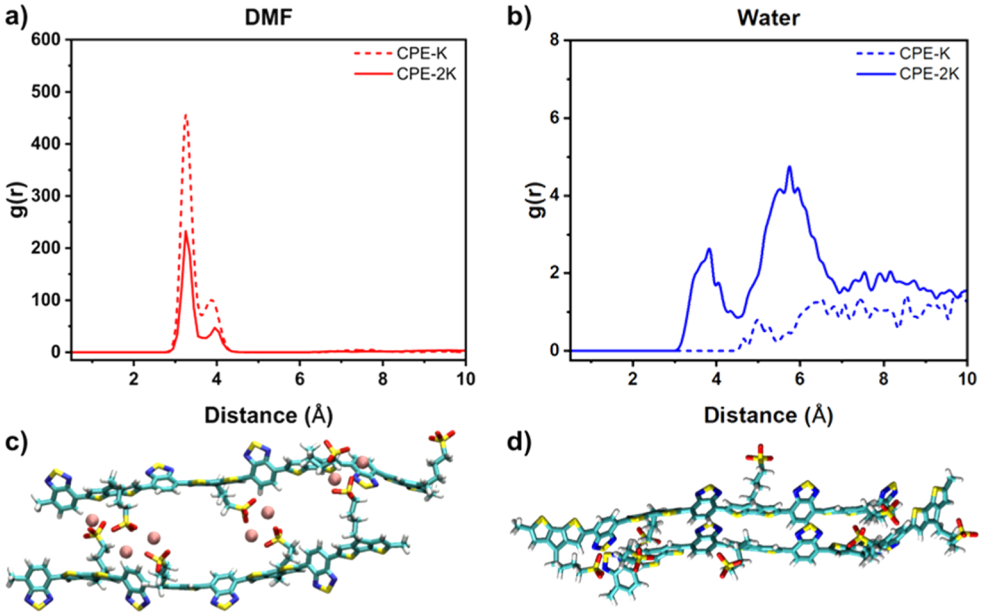

Figure 3. Radial distribution function between the K^+ cations and the sulfonate groups ($-SO_3^-$) of **CPE-K** and **CPE-2K** in DMF (a) and water (b) obtained from MD trajectories of a monomer. MD simulation snapshots of **CPE-K** tetramers in DMF (c) and water (d).

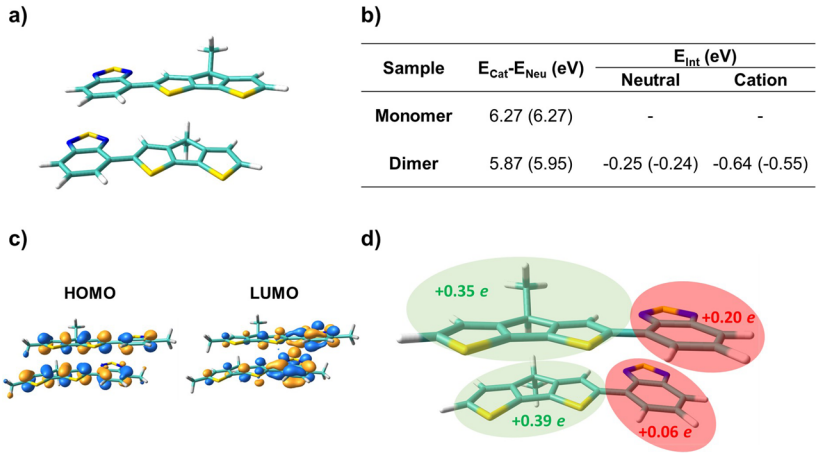

Sample	E_{Cat}-E_{Neu} (eV)	E_{Int} (eV)	
		Neutral	Cation
Monomer	6.27 (6.27)	-	-
Dimer	5.87 (5.95)	-0.25 (-0.24)	-0.64 (-0.55)

Figure 4. Lateral view of the DFT-calculated **CPE-K** dimer in a parallel configuration (a). DFT-calculated (PBE0-D3/6-31G**) ionization potentials (IP = $E_{Cat} - E_{Neu}$) and interaction energies E_{Int} ($E_{Int} = E_{dimer} - 2*E_{monomer}$ for the neutral dimer and $E_{Int} = E_{dimer}^{+} - E_{monomer} - E_{monomer}^{+}$ for the positively charged dimer) for the parallel (and antiparallel in brackets) **CPE-K** dimer (b). Frontier molecular orbitals of the parallel radical cation **CPE-K** dimer (c). DFT-calculated Mülliken atomic charge distribution in the parallel radical cation **CPE-K** dimer model (d).

3.1. Influence of Solvent Nature

Figures 2b and S2 show that, for both polymers, the intensity of the polaron band depends on the nature of the employed solvent or water/solvent mixture. Note that the ratio between the polaron and ICT peaks, $A_{Polaron}/A_{ICT}$, is higher in protic solvents (Table S1) such as H_2O or EtOH than in aprotic solvents (DMSO, DMF). To gain insights into this phenomenon, molecular dynamics (MD) simulations were carried out for a single **CPE-2K** monomer in water and DMF (Figure S5). These simulations revealed significant differences in the interaction of the countercation with the environment. In particular, the radial distribution function between K^+ ions and the sulfonate groups (Figure 3a,b) illustrates that when employing a solvent with a low dielectric constant, such as DMF, the countercation remains coordinated to the sulfonate. Conversely, in water, the K^+ countercations become solvated and diffuse freely throughout the system.

To further explore the effect of the countercation behavior on the intermolecular interactions when changing the solvent, MD simulations were performed in water and DMF also for systems made up of two tetramers of **CPE-K** or **CPE-2K** (Figure 3c,d). The obtained results show that in DMF, where the countercations maintain the coordination with the sulfonate groups, pairs of alkyl-ionic chains belonging to different tetramers are allowed to interact across the K^+ atoms, forming bridges that prevent the corresponding backbones from aggregating. Conversely, in water, the hydration of K^+ ion atoms prevents the formation of salt bridges, leading to an increased repulsion between alkyl sulfonate chains, which become straighter and more solvated, and allowing the backbones to π-stack. The hypothesis of the rupture of the salt bridges that suppress the stacking is supported experimentally by the precipitation of the proton-aggregated form after adding a proton source in DMF (see the Supporting Information). In line with these findings, in ref 26, XPS spectra

https://doi.org/10.1021/acs.chemmater.5c02392
Chem. Mater. 2026, 38, 808−818

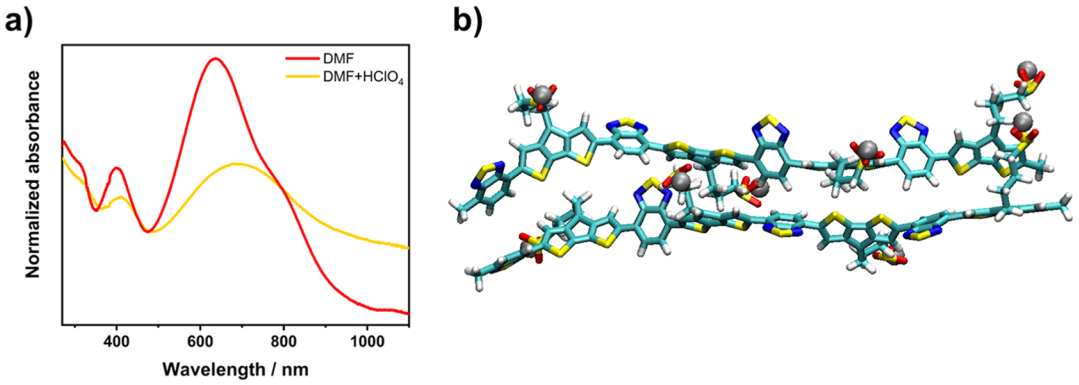

Figure 5. Experimental UV−vis spectra of **CPE-K** in DMF and DMF after adding 1 eq. of $HClO_4$ (a) and a snapshot taken from the MD simulation in DMF of two parallel **CPE-K** tetramers including $-HSO_3$ groups, with the hydrogen atoms bonded to sulfonate groups represented as gray spheres (b).

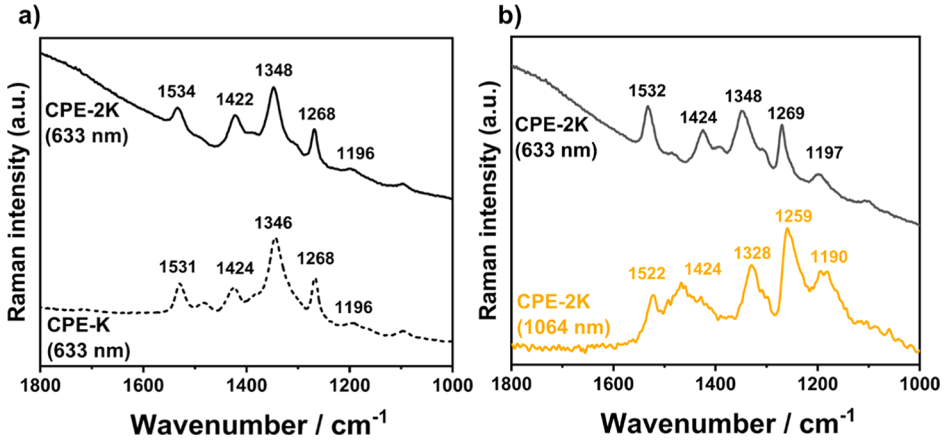

Figure 6. Solid-state Raman spectra of bulk **CPE-2K** and **CPE-K** at 633 nm (a) and the proton-aggregated form in DMF of **CPE-2K** at 633 and 1064 nm (b). These latter spectra are in resonance with the neutral and polaron band, respectively.

for the undoped species show the K^+ peak, which disappears after acid doping, confirming the ejection of the countercation.

It is evident that the distinct behavior exhibited by the counterions, which in turn depends on the nature of the solvent, exerts a direct influence on the intermolecular interactions, thereby either promoting or hindering aggregation of polymeric chains. The different availability of the countercations to form bridges between two polymer chains, due to the solvent nature, explains why the ratio ($A_{polaron}/A_{ICT}$) increases with the solvent polarity. The different ratios (especially in water) shown by **CPE-K** and **CPE-2K** can be mainly explained by the different numbers of alkylsulfonate chains per monomer (see the following sections).

The formation of polarons is promoted by this aggregation mechanism for the following reasons: (i) the polaron can now be stabilized by the possible delocalization across different polymeric chains. (ii) Aggregation facilitates the single-electron transfer step in the backbone protonation pathway due to the reduced interbackbone distance. Note that this process would be very unlikely to occur between fully solvated polymeric chains over large distances. This is in line with previously reported studies on porous self-doped conjugated polyelectrolytes, where it was shown that solid-state interactions have the potential to enhance interchain delocalization.[40]

To further investigate the role of aggregation in the polaron stability, DFT calculations were performed for parallel and antiparallel dimer models (Figures 4 and S9), with the aim of comparing the polaron stabilization with respect to the case of the isolated monomers. The energy difference of the radical cation compared to the neutral species decreases from 6.27 eV for the monomer to ∼5.90 eV for the dimer; therefore, the intermolecular interaction reduces the ionization potential by ∼0.4 eV. Interaction energy calculations show a ∼0.4 eV decrease as well, going from the neutral to the radical cation, indicating that, thanks to the increased charge delocalization, the polaron is more stabilized by aggregation than the neutral species. In line with this behavior, complete delocalization of the frontier orbitals is observed in the radical cation dimer (Figure 4c), while the Mülliken charge distribution shows that the polaron charge is shared by the two monomers (Figure 4d). These results clearly point out that π-stacking increases the thermodynamic stability of the charged species.

3.2. Influence of Adding a Proton Source

In the context of self-acid doping mechanisms, protonation within the backbone was proposed as a crucial factor in polaron formation.[29] However, as mentioned before, sp^2 aromatic carbons would have a low chance of protonation against sulfonate, and the resulting carbocation would exhibit a short lifetime, reducing the protonated species to a transient state. This consideration leads to the proposition that the introduction of an acid in the system mainly serves to displace the acid−base equilibrium that is inherent within the sulfonate group, as follows

https://doi.org/10.1021/acs.chemmater.5c02392
Chem. Mater. 2026, 38, 808−818

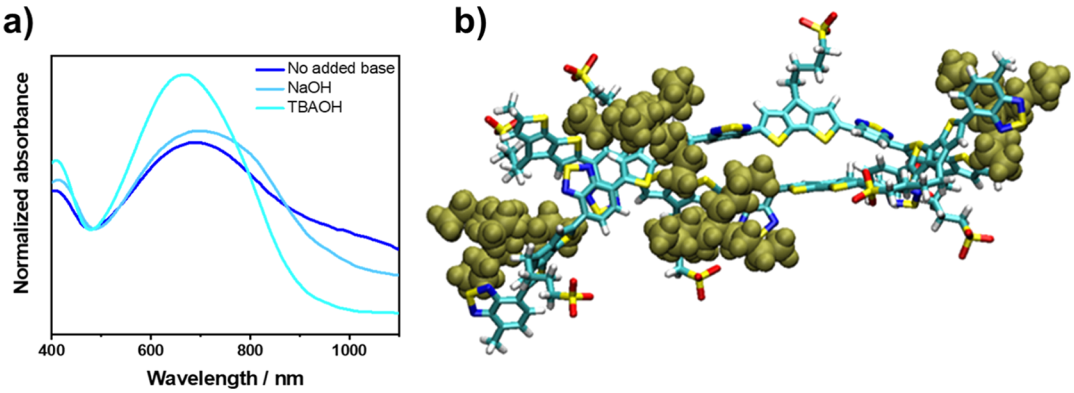

Figure 7. Experimental UV−vis spectra of **CPE-K** in pure water and after the addition of one equivalent of NaOH or TBAOH, respectively (a). MD snapshot of **CPE-K** showing TBA^+ in green (b).

$$R{-}SO_3^-K^+ + H^+ \rightleftharpoons R - HSO_3 + K^+ \quad (2)$$

To prove this hypothesis, stoichiometric amounts of $HClO_4$ were added to the samples in DMF. We found that the addition of only one equivalent of acid is sufficient to cause the appearance of the polaron band for both polymers (Figures 5 and S7). Furthermore, the formation of aggregates is observed after one night at 4 °C, for both **CPE-2K** and **CPE-K** (Figure S4).

To theoretically investigate the effect of protonating the sulfonates in DMF, we performed additional MD simulations. Initially, the system included both K^+ ions and sulfonates protonated by adding a positively charged hydrogen atom bonded to one sulfonate oxygen. After observing that bonded protons displaced countercations away from sulfonate groups, K^+ ions were removed to maintain the net charge neutrality of the simulation box.

Even though protonated sulfonate groups repel each other less than they do in the unprotonated form, the absence of K^+ prevented the alkyl-ionic chains from forming bridges. This can be attributed to the significantly smaller van der Waals radius of hydrogen compared to potassium. Following this, we infer that the addition of an acid in DMF is sufficient to cause the breakage of the K^+ ion bridges, thereby promoting π-stacking (see Figure 5b) and thus the formation of polarons.

Thus, these MD simulations suggest that the ultimate trigger of aggregation is the countercation behavior, which is modulated either from its solvation environment, as demonstrated in section 3.1, or from its displacement of the acid−base equilibrium, as discussed here.

To confirm the possible formation of polarons, the variation of the molecular structure of **CPE-2K** and **CPE-K** was assessed by Raman spectroscopy.[41,42] To this end, a comparison of the aggregates obtained after acid treatment in DMF and subsequent drying with respect to the bulk material was approached. As seen in Figure 6a, the two bulk polymers exhibit nearly identical Raman spectra, characterized by four main vibrational bands: at 1534 (1531) cm^{-1}, attributed to the C═C/C−C stretching of the benzothiadiazole (BT) unit; at 1422 (1424) cm^{-1}, associated with the C═C/C−C stretching of the cyclopentadithiophene (CPDT) unit; and at 1348 (1344) cm^{-1} and 1268 (1268) cm^{-1}, corresponding to the C−H wag of the BT and CPDT units, respectively. Additionally, a band at 1196 cm^{-1} is observed, which corresponds to the in-plane C−H wag of CPDT coupled with the symmetric C−H wag of BT. The calculated normal modes were key to the successful completion of this assignment (Figures S13 and S14).

In Figure 6b, Raman spectra of proton-aggregated **CPE-2K** are compared at excitation wavelengths of 633 and 1064 nm. At 633 nm, the neutral species are predominantly excited (cf. Figure 2), producing a spectrum identical to that of the bulk material. In contrast, excitation at 1064 nm selectively enters in resonance with polarons, showing a downshift of the principal normal modes and the increase of the C−H wag relative intensity with respect to the C═C/C−C stretches. This indicates a more delocalized π-conjugated skeleton resulting in quinoidization of the structure, as proved by the calculated bond length changes going from the neutral monomer to the radical cation (Figure S16). These results also indicate that a nontransitory protonation state of the backbone is absent as this would have resulted in a different Raman spectral profile, while the main molecular structural changes observed in our case are attributed to an aromatic → quinoid transformation of the π-conjugated skeleton ascribed to the cation formation.

3.3. Influence of Adding a Base

In a subsequent experiment, 1 equiv of NaOH was added to **CPE-K** and **CPE-2K** solutions in water. This resulted in a reduction in the intensity of polaron bands (~850−1100 nm). The incorporation of 1 equiv of a larger base, tetrabutylammonium hydroxide (TBAOH), results in a further substantial reduction of the polaron band intensity for both polymers (Figures 7a and S8). In the **CPE-K** spectrum, a shoulder at about 800 nm is particularly evident upon the addition of NaOH, but it is also present in DMF (Figure S3), though absent for **CPE-2K**. We hypothesize that it could be caused by the reduced symmetry of the **CPE-K** backbone, which contains only one alkyl-ionic side chain and one hydrogen. This asymmetry is a source of conformational disorder and a broader distribution of conjugation lengths with respect to **CPE-2K**. Note that the ratio between polaron and ICT peaks ($A_{polaron}/A_{ICT}$) of **CPE-2K** also decreases when adding NaOH and TBAOH (Table S2). To understand the origin of this effect, we performed MD simulations of tetramers in water, replacing the K^+ ion with TBA^+. TBA^+ is considerably bulkier than K^+ and consequently is less soluble in water. This results in TBA^+ ions remaining aggregated to the polymer instead of diffusing freely in water like K^+, as illustrated in Figure 7b, thereby hindering the stacking process to a greater extent than K^+.

We infer that, in contrast to the addition of $HClO_4$, the addition of stoichiometric quantities of NaOH increases the

https://doi.org/10.1021/acs.chemmater.5c02392
Chem. Mater. 2026, 38, 808−818

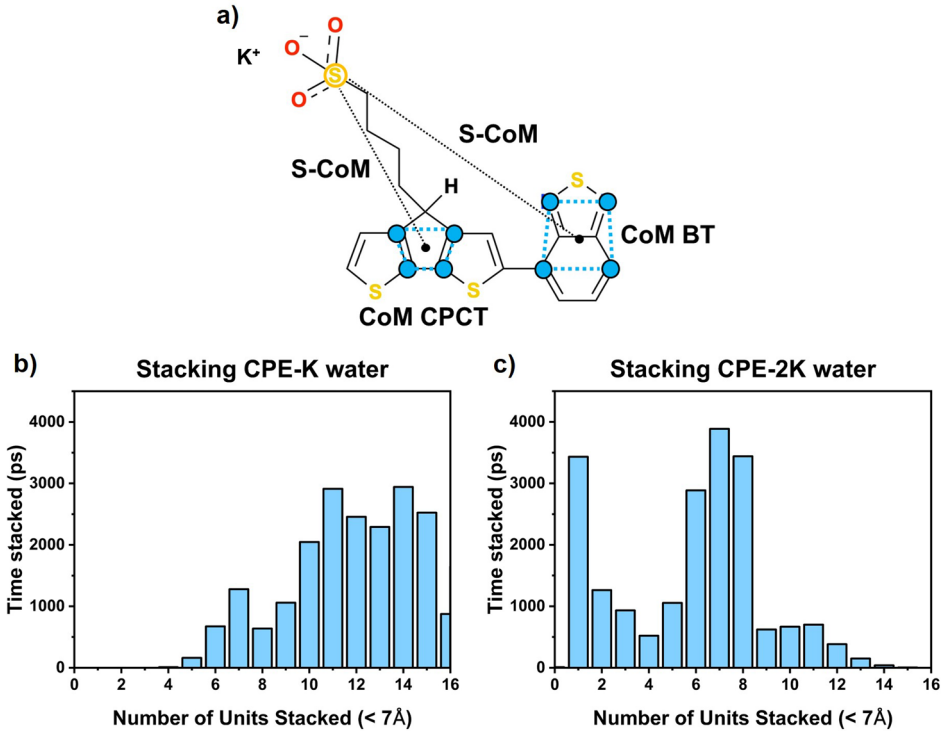

Figure 8. Definition of centers of mass (CoM) and S−CoM distance for **CPE-K** CPDT and BT units (a); number of intermolecular contacts (stacked units) over time during an MD simulation in water for two tetramers of **CPE-K** (b) and **CPE-2K** (c). Two units are considered in contact when the distance between two centers of mass is lower than 7 Å.

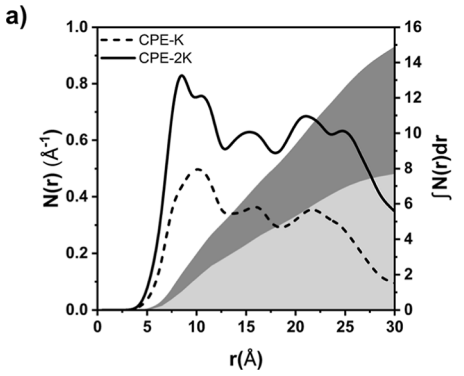

b)

System	Coulombic Stabilization (eV)
CPE-2K	-5.12 ± 0.31
CPE-K	-2.69 ± 0.11

Figure 9. Density $N(r)$ and number $\int N(r)r\,dr$ of sulfonate groups as a function of the distance from the backbone for **CPE-2K** and **CPE-K** (a) and total Coulombic stabilization for polarons localized on single monomers (b). Note that for our two tetramer systems the total number of butyl sulfonate chains is 8 for **CPE-K** and 16 for **CPE-2K**. Results are averaged over 10 simulations of two tetramers in water.

concentration of countercations around the polymeric chains. This displaces the acid−base equilibrium favoring the coordination of countercations with the sulfonate groups, allowing the alkyl−ionic chains to form salt bridges, which prevent aggregation and polaron formation. This effect is even stronger for bulkier and less soluble cations like TBA^+.

3.4. Influence of the Number of Alkyl Ionic Chains

The previous simulations linked polaron stability to the ease of aggregate formation (solvent, pH, or size of the countercation effect); however, the difference between **CPE-K** and **CPE-2K** seems unsolved because both CPEs share the same backbone. Visualization of the MD simulation trajectories in water and DMF revealed no significant differences between the two polymers, highlighting the necessity of quantitative indicators to elucidate the origin of the higher polaron stabilization in **CPE-2K**.

This issue was solved by analyzing the trajectory files obtained from ten MD simulations of **CPE-K** and **CPE-2K** polymers from different starting geometries in water (Figure S18). The analysis was performed by defining two centers of mass (CoM) per monomer, as shown in Figure 8a.

From these calculations, we retrieved information about the intermolecular contacts, with the aim of clarifying whether the reason for **CPE-2K** higher polaron stability is more efficient aggregation. To this end, we analyzed the number of BT and CPDT units stacked over time (Figure 8b,c), the average lifetime of these contacts, and the average angle between the aromatic planes of stacked units (Table S3). Interestingly, we observed that **CPE-K** presents a higher number of units stacked over time (Figure 8b,c), longer stacking lifetimes (3463 ps for **CPE-K** vs 2646 ps for **CPE-2K**), and a lower angle between stacked units (33° for **CPE-K** vs 37° for **CPE-**

https://doi.org/10.1021/acs.chemmater.5c02392
Chem. Mater. 2026, 38, 808−818

Scheme 2. Proposed Self-Doping Mechanism Based on Aggregation, Including the Following Steps: Alkyl-Ionic Bridges Hampering the Aggregation (a), Migration of the K^+ Countercations upon Proton Addition (b), Aggregated Structure after the Removal of K^+ (c), and Formation of the Polaronic State (d), Respectively

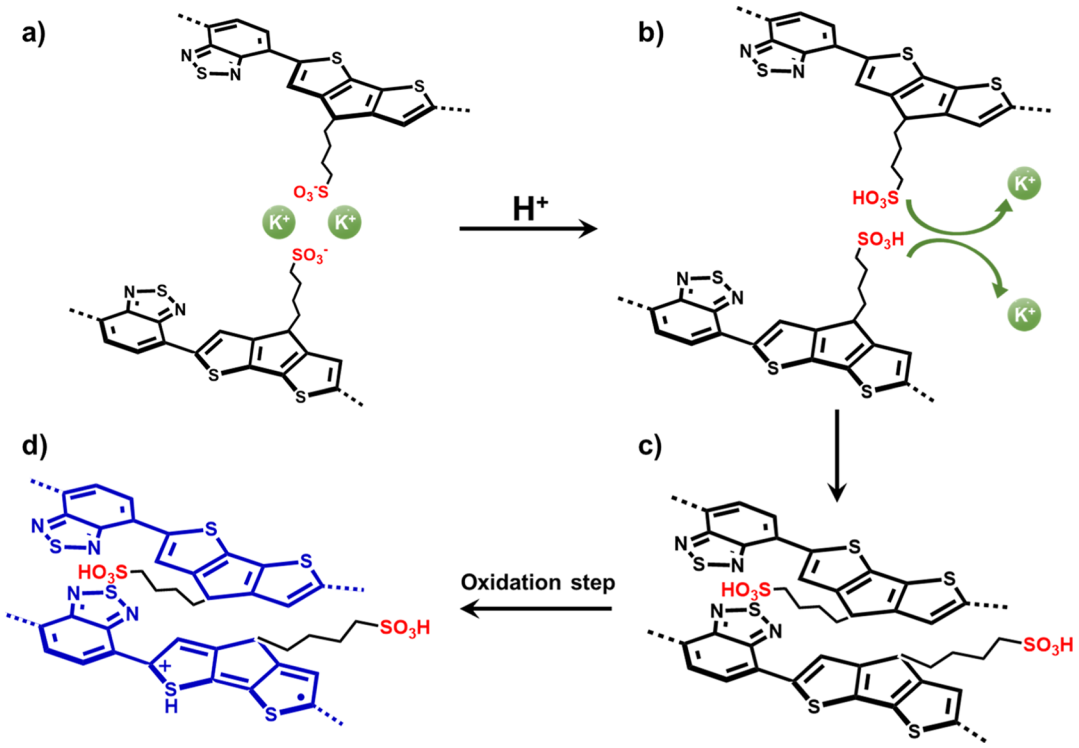

2K, see Table S3). All of these parameters indicate that **CPE-K** aggregates more effectively than **CPE-2K**. In contrast, for **CPE-2K**, it is more complicated to accommodate the two side chains without hampering the stacking.

These calculations can also provide us with valuable information regarding the Coulombic stabilization coming from the negative charges of the sulfonate groups. This, in turn, may help explain the higher polaron stability of **CPE-2K**. Note that this polymer has an extra negative charge per monomer with respect to **CPE-K**, which can, in principle, help further stabilize the positive charge in the backbone and promote the formation of the polaron. For that, we computed the density of CoM−Sulfonate pairs (S−CoM) over distance ($N(r)$), the total number of sulfonates around a given backbone center up to a certain distance ($\int_o^r N(r')\mathrm{d}r'$), and the total Coulombic stabilization (from the inverse of all S−CoM distances). All of these parameters were calculated for ten MD simulations with aleatory starting points for two tetramers of **CPE-K** and **CPE-2K** in water.

CPE-2K contains twice the number of sulfonated groups than **CPE-K**, logically resulting in a higher number of CPDT- and BT-sulfonate pairs. However, the higher number of sulfonate groups in **CPE-2K** does not, by itself, guarantee greater stabilization. This enhancement occurs only when the additional groups are positioned close enough to the backbone to form short-range sulfonate-backbone contacts, a condition that is influenced by the degree of aggregation. As seen in Figure 9, $N(r)$ and $\int N(r)r\,\mathrm{d}r$ plots both show that **CPE-2K** has more CoM−S pairs but also that the number of pairs increases much more rapidly than for **CPE-K**.

The different number and spatial distribution of the CoM−S pairs result in electrostatic stabilization energies of −2.69 eV for **CPE-K** and −5.12 eV for **CPE-2K** per monomer. These energies were calculated for a hypothetical point positive charge located either at the CPDT or at BT centers (see the Experimental and Computational Methods section). Notably, the second value almost matches the gas phase ionization potential of a **CPE-2K** aggregated dimer without side chains (Figure 4). Therefore, we conclude that, although **CPE-K** aggregates more easily, **CPE-2K** displays a higher polaron concentration in water owing to the larger stabilization of the extra charges by Coulomb interaction with the surrounding sulfonate groups, which, in turn, is enhanced by aggregation that increases the number of sulfonate groups that can eventually stabilize a polaron on a given monomeric unit.

The electrochemical responses of the two polymers corroborate the aforementioned results (Figure S17): they are characterized by low oxidation potentials. In particular, **CPE-2K** has a lower oxidation potential than **CPE-K** (see the table in Figure S17).

3.5. Self-Doping Mechanism Proposed

Following a thorough review of the experimental and theoretical results that have been discussed, we are now in a position to revisit the self/self-acid doping mechanism of this family of CPEs (Scheme 1). There are still open questions regarding this mechanism, such as the instability of the protonated backbone and the role of aggregation. Specifically, we propose an initial step, prior to the oxidation, in which the behavior of countercations drives the aggregation (Scheme 2).

As a starting point, we consider a solution prepared with DMF, where countercations coordinate with sulfonate groups, forming alkyl-ionic bridges, as demonstrated in Figure 3 and sketched in Scheme 2a. When an acid is added, sulfonate groups become protonated, moving away countercations (Scheme 2b). This displacement disrupts the alkyl−ionic

https://doi.org/10.1021/acs.chemmater.5c02392
Chem. Mater. 2026, 38, 808−818

bridges, facilitating π-stacking between PCPDTBT units and thereby inducing aggregation (Scheme 2c).

At this stage, several reaction paths become available to form a polaron (Scheme 2d), including a redox reaction with atmospheric oxygen, or with Cl^{7+} of $HClO_4$, or the previously reported backbone protonation mechanism where now single-electron transfer is more likely thanks to the short interbackbone distances allowed by the aggregation. Indeed, cyclic voltammetry measurements (Figure S17) indicate a low oxidation potential for **CPE-2K** (0.1 V), thereby confirming the accessibility of the redox reaction for all of these possible paths.

If a solvent with a significant dielectric constant (such as water) is used, the metallic countercations are solvated, thus preventing the formation of salt bridges and promoting polymer aggregation. Regarding electrochemical self-doping (Scheme 2a), this can be considered as a similar process driven by a different trigger; in this case, it is the applied potential, rather than the addition or removal of protons, that drives the ion exchange mechanism.

4. CONCLUSIONS

In this investigation, several unclear aspects of the self-doping mechanism in polyconjugated electrolytes were addressed by a combination of various experimental techniques and molecular dynamics simulations. It has been demonstrated that the polaron thermodynamic stability is enhanced by two intertwined factors: Coulombic stabilization and aggregation. It was also revealed that π-stacking between polymer chains is hindered in apolar solvents due to the insolubility of K^+ countercations and the formation of sulfonate−cation−sulfonate salt bridges.

A more comprehensive understanding of the self-doping mechanism has been proposed, with aggregation being identified as the primary factor in differentiating various doping levels in relation to solvent polarity, concentration, and pH. These factors are all influenced by countercation behavior, which either facilitates or hinders the formation of K^+ bridges between polymers.

It is interesting to note that in addition to aggregation the enhanced polaron stabilization of **CPE-2K** compared to that of **CPE-K** can be explained by Coulombic stabilization. It is evident that the presence of an additional alkyl ionic chain per unit results in a substantial enhancement of Coulombic stabilization, consequently promoting enhanced polaron stability.

Overall, the present work has expanded the previous understanding of the self-/self-acid-doping mechanism by including the aggregation causes and its effects. This comprehensive approach provides a more profound understanding of the phenomenon of self-doping in conjugated polyelectrolytes and the fundamental driving factors behind it.

■ ASSOCIATED CONTENT

Supporting Information

The Supporting Information is available free of charge at https://pubs.acs.org/doi/10.1021/acs.chemmater.5c02392.

Supplementary figures and tables, synthetic details, UV−vis data, and theoretical calculations (PDF)

■ AUTHOR INFORMATION

Corresponding Authors

M. Carmen Ruiz Delgado − *Departamento De Química Física, Universidad De Málaga, Málaga ES-29071, Spain; Instituto Universitario De Materiales y Nanotecnología, IMANA, University of Malaga, Malaga ES-29071, Spain;* orcid.org/0000-0001-8180-7153; Email: carmenrd@uma.es

Luca Muccioli − *Dipartimento Di Chimica Industriale "Toso Montanari", Università Di Bologna, Bologna IT-40136, Italy;* orcid.org/0000-0001-9227-1059; Email: luca.muccioli@unibo.it

Barbara Vercelli − *Istituto di Chimica Della Materia Condensata e di Tecnologie per L'Energia CNR-ICMATE, Milano IT-20125, Italy;* orcid.org/0000-0003-1549-7032; Email: barbara.vercelli@cnr.it

Authors

Fernando Muñoz-Alba − *Departamento De Química Física, Universidad De Málaga, Málaga ES-29071, Spain; Instituto Universitario De Materiales y Nanotecnología, IMANA, University of Malaga, Malaga ES-29071, Spain*

Lorenzo Soprani − *Dipartimento Di Chimica Industriale "Toso Montanari", Università Di Bologna, Bologna IT-40136, Italy*

Benedetta Maria Squeo − *Istituto di Scienze e Tecnologie Chimiche "Giulio Natta" CNR-SCITEC, Milano IT-20133, Italy*

Mariacecilia Pasini − *Istituto di Scienze e Tecnologie Chimiche "Giulio Natta" CNR-SCITEC, Milano IT-20133, Italy*

Raúl González-Núñez − *Departamento De Química Física, Universidad De Málaga, Málaga ES-29071, Spain; Instituto Universitario De Materiales y Nanotecnología, IMANA, University of Malaga, Malaga ES-29071, Spain;* orcid.org/0000-0003-0170-8492

Rocío Ponce Ortiz − *Departamento De Química Física, Universidad De Málaga, Málaga ES-29071, Spain; Instituto Universitario De Materiales y Nanotecnología, IMANA, University of Malaga, Malaga ES-29071, Spain;* orcid.org/0000-0002-3836-3494

Complete contact information is available at: https://pubs.acs.org/10.1021/acs.chemmater.5c02392

Notes

The authors declare no competing financial interest.

■ ACKNOWLEDGMENTS

This research was funded by the MICINN/AEI/10.13039/501100011033 (Project PID2022-139548NB-I00) and Junta de Andalucía (FQM-159). B.V. kindly acknowledges the Italian Government for the financial support and CNR for the Short-Term Mobility Grant (STM 2020). The authors thank David Beljonne (University of Mons) and Giacomo Londi (University of Pisa) for useful discussions. The authors would also like to thank the computer resources, technical expertise, and assistance provided by the SCBI (Supercomputing and Bioinformatics) center and the vibrational spectroscopy (EVI) lab of the Research Central Services (SCAI) of the University of Málaga. Funding for open access charge: Universidad de Málaga/CBUA.

REFERENCES

(1) Shi, S.; Wudl, F. Synthesis and Characterization of a Water-Soluble Poly(p-Phenylenevinylene) Derivative. *Macromolecules* **1990**, *23* (8), 2119−2124.

(2) Patil, A. O.; Ikenoue, Y.; Wudl, F.; Heeger, A. J. Water Soluble Conducting Polymers. *J. Am. Chem. Soc.* **1987**, *109* (6), 1858−1859.

(3) Wan, Y.; Zhang, X.; Bazan, G. C.; Nguyen, T. Q.; Lu, G. Polarons in Conjugated Polyelectrolytes: A First-Principles Perspective. *Adv. Funct. Mater.* **2022**, *32* (52), 2209394.

(4) Shin, Y. C.; Lee, J. H.; Jeong, J. E.; Kim, B.; Lee, E. J.; Jin, O. S.; Jung, T. G.; Lee, J. J.; Woo, H. Y.; Han, D. W. Cell imaging and DNA delivery in fibroblastic cells by conjugated polyelectrolytes. *Biotechnol. Appl. Biochem.* **2013**, *60* (6), 580−588.

(5) Fidanovski, K.; Gu, M.; Travaglini, L.; Lauto, A.; Mawad, D. Self-Doping and Self-Acid-Doping of Conjugated Polymer Bioelectronics: The Case for Accuracy in Nomenclature. *Adv. Healthcare Mater.* **2023**, *13*, 2302354.

(6) Cox-Vázquez, S. J.; Shakir, B.; Medrano, O.; Shah, D.; Bortey, K.; Biswas, B.; Tran, A.; Tran, C.; Vázquez, R. J. Advancements and Applications of Conjugated Polyelectrolytes and Conjugated Oligoelectrolytes in Bioanalytical and Electrochemical Contexts. *JACS Au* **2024**, *4* (12), 4592−4611.

(7) Kang, Q.; Liao, Q.; Xu, Y.; Xu, L.; Zu, Y.; Li, S.; Xu, B.; Hou, J. P-Doped Conducting Polyelectrolyte as an Anode Interlayer Enables High Efficiency for 1 Cm 2 Printed Organic Solar Cells. *ACS Appl. Mater. Interfaces* **2019**, *11* (22), 20205−20213.

(8) Han, Y. W.; Choi, J. Y.; Lee, Y. J.; Ko, E. J.; Choi, M. H.; Suh, I. S.; Moon, D. K. Organic Solar Cells: Vertical Phase Separation for Highly Efficient Organic Solar Cells Incorporating Conjugated-Polyelectrolytes (Adv. Mater. Interfaces 3/2019). *Adv. Mater. Interfaces* **2019**, *6* (3), 1970018.

(9) Bi, S.; Leng, X.; Li, Y.; Zheng, Z.; Zhang, X.; Zhang, Y.; Zhou, H. Interfacial Modification in Organic and Perovskite Solar Cells. *Adv. Mater.* **2019**, *31* (45), 1805708.

(10) Moon, S.; Khadtare, S.; Wong, M.; Han, S.-H.; Bazan, G. C.; Choi, H. Hole Transport Layer Based on Conjugated Polyelectrolytes for Polymer Solar Cells. *J. Colloid Interface Sci.* **2018**, *518*, 21−26.

(11) Kim, S.; Jeong, J.-E.; Hong, J.; Lee, K.; Lee, M. J.; Woo, H. Y.; Hwang, I. Improved Interfacial Crystallization by Synergic Effects of Precursor Solution Stoichiometry and Conjugated Polyelectrolyte Interlayer for High Open-Circuit Voltage of Perovskite Photovoltaic Diodes. *ACS Appl. Mater. Interfaces* **2020**, *12* (10), 12328−12336.

(12) Hoven, C. V.; Garcia, A.; Bazan, G. C.; Nguyen, T. Recent Applications of Conjugated Polyelectrolytes in Optoelectronic Devices. *Adv. Mater.* **2008**, *20* (20), 3793−3810.

(13) Zhou, H.; Zhang, Y.; Mai, C.-K.; Seifter, J.; Nguyen, T.-Q.; Bazan, G. C.; Heeger, A. J. Solution-Processed PH-Neutral Conjugated Polyelectrolyte Improves Interfacial Contact in Organic Solar Cells. *ACS Nano* **2015**, *9* (1), 371−377.

(14) Zhou, H.; Zhang, Y.; Mai, C.; Collins, S. D.; Bazan, G. C.; Nguyen, T.; Heeger, A. J. Polymer Homo-Tandem Solar Cells with Best Efficiency of 11.3%. *Adv. Mater.* **2015**, *27* (10), 1767−1773.

(15) Lassi, E.; Squeo, B. M.; Sorrentino, R.; Scavia, G.; Mrakic-Sposta, S.; Gussoni, M.; Vercelli, B.; Galeotti, F.; Pasini, M.; Luzzati, S. Sulfonate-Conjugated Polyelectrolytes as Anode Interfacial Layers in Inverted Organic Solar Cells. *Molecules* **2021**, *26* (3), 763.

(16) Luo, J.; Wu, H.; He, C.; Li, A.; Yang, W.; Cao, Y. Enhanced Open-Circuit Voltage in Polymer Solar Cells. *Appl. Phys. Lett.* **2009**, *95* (4), 043301.

(17) Lee, S.; Jang, C. H.; Nguyen, T. L.; Kim, S. H.; Lee, K. M.; Chang, K.; Choi, S. S.; Kwak, S. K.; Woo, H. Y.; Song, M. H. Conjugated Polyelectrolytes as Multifunctional Passivating and Hole-Transporting Layers for Efficient Perovskite Light-Emitting Diodes. *Adv. Mater.* **2019**, *31* (24), 1900067.

(18) Lee, W.; Seo, J. H.; Woo, H. Y. Conjugated Polyelectrolytes: A New Class of Semiconducting Material for Organic Electronic Devices. *Polym.* **2013**, *54* (19), 5104−5121.

(19) Lee, B. H.; Jung, I. H.; Woo, H. Y.; Shim, H.; Kim, G.; Lee, K. Multi-Charged Conjugated Polyelectrolytes as a Versatile Work Function Modifier for Organic Electronic Devices. *Adv. Funct. Mater.* **2014**, *24* (8), 1100−1108.

(20) Sun, M.; Lan, L.; Wang, L.; Peng, J.; Cao, Y. Synthesis of Novel Conjugated Polyelectrolytes for Organic Field-Effect Transistors Gate Dielectric Materials. *Macromol. Chem. Phys.* **2008**, *209* (24), 2504−2509.

(21) Seo, J. H.; Gutacker, A.; Walker, B.; Cho, S.; Garcia, A.; Yang, R.; Nguyen, T.-Q.; Heeger, A. J.; Bazan, G. C. Improved Injection in N-Type Organic Transistors with Conjugated Polyelectrolytes. *J. Am. Chem. Soc.* **2009**, *131* (51), 18220−18221.

(22) Mai, C.-K.; Russ, B.; Fronk, S. L.; Hu, N.; Chan-Park, M. B.; Urban, J. J.; Segalman, R. A.; Chabinyc, M. L.; Bazan, G. C. Varying the Ionic Functionalities of Conjugated Polyelectrolytes Leads to Both P- and n-Type Carbon Nanotube Composites for Flexible Thermoelectrics. *Energy Environ. Sci.* **2015**, *8* (8), 2341−2346.

(23) Kee, S.; Haque, M. A.; Lee, Y.; Nguyen, T. L.; Rosas Villalva, D.; Troughton, J.; Emwas, A.-H.; Alshareef, H. N.; Woo, H. Y.; Baran, D. A Highly Conductive Conjugated Polyelectrolyte for Flexible Organic Thermoelectrics. *ACS Appl. Energy Mater.* **2020**, *3* (9), 8667−8675.

(24) Lee, W.; Chouhan, J. L.; Harit, A. K.; Park, C.; Kim, D.; McCuskey, S. R.; Bazan, G. C.; Woo, H. Y. Emerging Potential of Conjugated Polyelectrolytes beyond Boundaries. *ACS Nano* **2025**, *19* (6), 5938−5965.

(25) Mai, C.; Zhou, H.; Zhang, Y.; Henson, Z. B.; Nguyen, T.; Heeger, A. J.; Bazan, G. C. Facile Doping of Anionic Narrow-Band-Gap Conjugated Polyelectrolytes During Dialysis. *Angew. Chem., Int. Ed.* **2013**, *52* (49), 12874−12878.

(26) Cao, D. X.; Leifert, D.; Brus, V. V.; Wong, M. S.; Phan, H.; Yurash, B.; Koch, N.; Bazan, G. C.; Nguyen, T.-Q. The Importance of Sulfonate to the Self-Doping Mechanism of the Water-Soluble Conjugated Polyelectrolyte PCPDTBT-SO 3 K. *Mater. Chem. Front.* **2020**, *4* (12), 3556−3566.

(27) Ikenoue, Y.; Chiang, J.; Patil, A. O.; Wudl, F.; Heeger, A. J. Verification of the "Cation-Popping" Doping Mechanism of Self Doped Polymers. *J. Am. Chem. Soc.* **1988**, *110* (9), 2983−2985.

(28) Ikenoue, Y.; Saida, Y.; Kira, M.-A.; Tomozawa, H.; Yashima, H.; Kobayashi, M. A Facile Preparation of a Self-Doped Conducting Polymer. *J. Chem. Soc. Chem. Commun.* **1990**, No. 23, 1694.

(29) Chen, S. A.; Hua, M. Y. Structure and Doping Level of the Self-Acid-Doped Conjugated Conducting Polymers: Poly[n-(3′-Thienyl)-Alkanesulfonic Acids]. *Macromolecules* **1993**, *26* (25), 7108−7110.

(30) Marqués, P. S.; Londi, G.; Yurash, B.; Nguyen, T.-Q.; Barlow, S.; Marder, S. R.; Beljonne, D. Understanding How Lewis Acids Dope Organic Semiconductors: A "Complex" Story. *Chem. Sci.* **2021**, *12* (20), 7012−7022.

(31) Yurash, B.; Cao, D. X.; Brus, V. V.; Leifert, D.; Wang, M.; Dixon, A.; Seifrid, M.; Mansour, A. E.; Lungwitz, D.; Liu, T.; Santiago, P. J.; Graham, K. R.; Koch, N.; Bazan, G. C.; Nguyen, T.-Q. Towards Understanding the Doping Mechanism of Organic Semiconductors by Lewis Acids. *Nat. Mater.* **2019**, *18* (12), 1327−1334.

(32) Feller, S. E.; Zhang, Y.; Pastor, R. W.; Brooks, B. R. Constant Pressure Molecular Dynamics Simulation: The Langevin Piston Method. *J. Chem. Phys.* **1995**, *103* (11), 4613−4621.

(33) Phillips, J. C.; Hardy, D. J.; Maia, J. D. C.; Stone, J. E.; Ribeiro, J. V.; Bernardi, R. C.; Buch, R.; Fiorin, G.; Hénin, J.; Jiang, W.; McGreevy, R.; Melo, M. C. R.; Radak, B. K.; Skeel, R. D.; Singharoy, A.; Wang, Y.; Roux, B.; Aksimentiev, A.; Luthey-Schulten, Z.; Kalé, L. V.; Schulten, K.; Chipot, C.; Tajkhorshid, E. Scalable Molecular Dynamics on CPU and GPU Architectures with NAMD. *J. Chem. Phys.* **2020**, *153* (4), 044130.

(34) Essmann, U.; Perera, L.; Berkowitz, M. L.; Darden, T.; Lee, H.; Pedersen, L. G. A Smooth Particle Mesh Ewald Method. *J. Chem. Phys.* **1995**, *103* (19), 8577−8593.

(35) Vanommeslaeghe, K.; Hatcher, E.; Acharya, C.; Kundu, S.; Zhong, S.; Shim, J.; Darian, E.; Guvench, O.; Lopes, P.; Vorobyov, I.; Mackerell, A. D. CHARMM General Force Field: A Force Field for Drug-like Molecules Compatible with the CHARMM All-atom

Additive Biological Force Fields. *J. Comput. Chem.* **2010**, *31* (4), 671−690.
(36) Grimme, S.; Ehrlich, S.; Goerigk, L. Effect of the Damping Function in Dispersion Corrected Density Functional Theory. *J. Comput. Chem.* **2011**, *32* (7), 1456−1465.
(37) Adamo, C.; Barone, V. Toward Reliable Density Functional Methods without Adjustable Parameters: The PBE0Model. *J. Chem. Phys.* **1999**, *110* (13), 6158−6170.
(38) Francl, M. M.; Pietro, W. J.; Hehre, W. J.; Binkley, J. S.; Gordon, M. S.; Defrees, D. J.; Pople, J. A. Self - Consistent Molecular Orbital Methods. XXIII. A Polarization - Type Basis Set for Second - Row Elements. *J. Chem. Phys.* **1982**, *77*, 3654−3665.
(39) Cox, S. R.; Williams, D. E. Representation of the Molecular Electrostatic Potential by a Net Atomic Charge Model. *J. Comput. Chem.* **1981**, *2* (3), 304−323.
(40) Medrano, O.; Zhou, Q.; Shakir, B.; Narváez-Lozano, G. A.; Hickey, E.; Bayro, M. J.; Bloch, E. D.; Vázquez, R. J. Porous and Self-Doped Conjugated Polyelectrolytes Exhibiting Open-Shell Character and Dual Ion-Electron Conduction. *Chem. Mater.* **2025**, *37* (16), 6282−6292.
(41) Mosca, S.; Milani, A.; Castiglioni, C.; Hernández Jolín, V.; Meseguer, C.; López Navarrete, J. T.; Zhao, C.; Sugiyasu, K.; Ruiz Delgado, M. C. Raman Fingerprints of π-Electron Delocalization in Polythiophene-Based Insulated Molecular Wires. *Macromolecules* **2022**, *55* (9), 3458−3468.
(42) Gámez-Valenzuela, S.; Comí, M.; González, S. R.; Delgado, M. C. R.; Al-Hashimi, M.; Ponce Ortiz, R. The Fluorination Effect: The Importance of Backbone Planarity in Achieving High Performance Ambipolar Field Effect Transistors. *J. Mater. Chem. C* **2023**, *11* (24), 8027−8036.

https://doi.org/10.1021/acs.chemmater.5c02392
Chem. Mater. 2026, 38, 808−818